ADVANCED FUNCTIONAL MATERIALS
www.afm-journal.de

Rational Tailored Polyfluorosubstituted Amide Molecule for Stabilizing PbI_6 Framework and Inhibiting Ion Migration Toward Highly Efficient and Stable Perovskite Solar Cells

Shidong Cai, Jie Gao, Yongjing Wu, Yaqing Zou, Jiading Liang, Yaoyao Li, Xiafeng He, Qingrui Cai, Mingliang Wang, Xiaozhen Huang, Xuran Wang, Sajid Sajid, Dong Wei, Ruidan Zhang,* Dandan Song,* and Yang Wang**

Perovskite solar cells (PSCs), while highly efficient, face stability challenges that hinder their commercial application. These instability issues mainly arise from the fragile nature of Pb—I bonds in perovskites, which easily break under environmental stresses such as heat and light, leading to the breakdown of the [PbI_6] framework and irreversible degradation. To address these issues, a multifunctional molecule, N^1,N^4-bis(2,3,5,6-tetrafluoro-4-iodophenyl)terephthalamide (FIPh-A), is designed and synthesized to enhance the stability of perovskite films and devices. FIPh-A molecule possesses carbonyl, amino, and iodotetrafluorophenyl groups that bind and stabilize Pb^{2+} ions and $[PbI_6]^{4-}$ octahedra structure, preventing ion migration in perovskite films. The activation energy of ion migration increases obviously from 0.28 eV to 0.39 eV by adding FIPh-A verified by experiment results. The residual strain is also released efficiently by introducing FIPh-A molecule into perovskite films characterized by grazing incidence X-ray diffraction. The champion PSC with FIPh-A achieves a power conversion efficiency of 24.60%. After 500 h of continuous illumination (ISOS-L-1) and 300 h of thermal aging at 80 °C (ISOS-D-2I), these PSCs with FIPh-A maintained 93% and 77% of their initial efficiency, respectively. These results emphasize the potential of multifunctional additives in overcoming the stability challenges of PSCs, thereby facilitating their commercial advancement.

1. Introduction

Perovskite solar cells (PSCs) have demonstrated a rapid increase in photovoltaic conversion efficiency (PCE), surging from 3.8% to an impressive 26.1%,[1–13] thereby affirming as a highly promising candidate for commercial next-generation thin-film photovoltaic applications. However, perovskite materials have a soft lattice structure that can easily distort and allow ions to move when exposed to continuous light or a thermal environment. Such structural weakness greatly reduces the stability of perovskite films and devices, presenting a major obstacle to their commercial development. The instability primarily arises from the fragility of Pb—I bonds in perovskite materials, which are susceptible to breaking under external stresses such as heat and light.[14–17] The breaking of these bonds leads to the disintegration of the PbI_6 framework and the subsequent release of iodide ions (I^-). Under continuous illumination, these I^- ions can

S. Cai, J. Gao, Y. Wu, X. He, Q. Cai, M. Wang, D. Wei, R. Zhang
College of Physics and Energy
Fujian Normal University
Fuzhou, Fujian 350117, P. R. China
E-mail: q397983012@126.com; rdzhang@fjnu.edu.cn

Y. Zou, X. Huang, X. Wang, Y. Wang
Strait Institute of Flexible Electronics (SIFE, Future Technologies)
Fujian Key Laboratory of Flexible Electronics
Fujian Normal University and Strait Laboratory of Flexible Electronics (SLoFE)
Fuzhou, Fujian 350117, P. R. China
E-mail: ifewangy@fjnu.edu.cn

J. Liang, Y. Li, D. Song
Key Lab Luminescence & Opt Informat
Beijing Jiaotong University
Minist Educ
Beijing 100044, P. R. China
E-mail: ddsong@bjtu.edu.cn

S. Sajid
Department of Chemical and Petroleum Engineering
United Arab Emirates University
P.O.Box, Al Ain 15551, UAE

The ORCID identification number(s) for the author(s) of this article can be found under https://doi.org/10.1002/adfm.202411014

DOI: 10.1002/adfm.202411014

migrate and oxidize into iodine molecules I_2($2I^- = I_2 + 2e^-$).[16–18,19] As temperatures rise, these I_2 molecules are likely to volatilize, creating numerous lead (Pb^0) defects within the perovskite films($PbI_2 = Pb^0 + I_2$).[20] Moreover, I_2 can react with metal electrodes, such as Au and Ag, causing irreversible degradation at the transport layer interface of PSCs.[21,22] Essentially, the migration of I^- ions create many deep-level defects in the perovskite films and interfaces, which accelerates the degradation of both the films and devices.

Therefore, developing effective strategies to reduce I^- migration and loss is crucial for improving the stability of perovskite films and devices, and facilitating the commercialization of PSCs. Currently, two main methods have been proven to inhibit I^- ion migration: one is using additives that capture iodine ions. For example, Zhou et al. utilized starch-I supramolecules as "iodine buffers" in PSCs, retaining sufficient iodine within the perovskite to inhibit ion drift and repair iodine vacancies.[23] Similarly, He et al. employed perfluoro dodecyl iodide, which can capture and bind I_x^- through halogen bonding due to its directed I_x^- affinity.[24] Fang et al. introduced β-cyclodextrin (β-CD) iodine traps to capture iodine produced within the perovskite and prevent its escape.[25] Huang et al. also reported the introduction of the reducing agent benzyhydrazine hydrochloride (BHC) into the perovskite precursor solution, which induces the reduction of I_2 to I^- both in solution and in the film state.[26] The other method involves the use of multifunctional additives with electron-donor and proton-donor functional sites, such as amides and carboxylic groups, which have been shown to anchor Pb—I units and stabilize the Pb—I frameworks. For instance, Pang et al. proposed a stabilization strategy for PbI_6 octahedra. Introducing a conjugated structure into amides significantly enhances their ability to anchor Pb—I units, reducing ion migration channels.[27] Liu et al. incorporated 2,2-difluoromalondiamide into the perovskite layer, providing substantial support to the Pb—I framework and significantly suppressing defect density and ion migration.[28] These methods have demonstrated that molecular interactions provided by additives can effectively inhibit I^- migration and loss, contributing to the stability of perovskite films and devices.

In this study, we designed and synthesized a novel multifunctional additive, N^1,N^4-bis(2,3,5,6-tetrafluoro-4-iodophenyl)terephthalamide (FIPh-A), with benzamide and symmetric iodotetrafluorophenyl groups. Density functional theory (DFT) calculation showed that the carbonyl group (C═O) and fluorine (F) atom in FIPh-A can interact with Pb^{2+} ions, while its amine group forms hydrogen bonds with I^-, synergistically stabilizing the PbI_6 framework. Furthermore, its iodotetrafluorophenyl group captures and anchors I^- through halogen bond donors (-C—I), suppressing I^- loss and migration. Spectral and electrochemical analyses confirmed these effects, demonstrating an obvious increase in activation energy for ion migration. Grazing incidence X-ray diffraction (GIXRD) characterization also revealed that FIPh-A enhances the crystalline quality of the film by alleviating residual strain. As a result, PSCs with FIPh-A achieved a PCE of 24.60%. After 500 h of continuous illumination (ISOS-L-1) and 300 h thermal aging at 80 °C (ISOS-D-2I), these PSCs maintained 93% and 77% of their initial efficiency, respectively.

2. Results and Discussion

To verify the interactions between FIPh-A and perovskites and elucidate the mechanism behind its impact on I^- migration and loss, we employed a combination of DFT calculations and experimental methods to characterize perovskite films both with FIPh-A and without FIPh-A (control). As illustrated in **Figure 1a**, the molecular structure of FIPh-A and its electrostatic potential (ESP) distribution are depicted. The electron-rich region near the carbonyl (C═O) group and F atom (shown in red in Figure 1a) indicates potential coordination with Pb^{2+} cations in the perovskite lattice. The electron-deficient regions near the amino (-NH) group (shown in blue in Figure 1a) and the halogen bonding sites on the iodotetrafluorophenyl moiety suggest potential interactions with iodide anions within the perovskite structure.[29]

The low formation energy of iodine vacancies often results in their considerable presence during device operation, thereby increasing defect density and promoting the migration of I^- ions. This ion migration causes stoichiometric polarization and accelerates the undesirable segregation of iodine-rich phases in perovskites,[30,31] which act as traps, capturing nearby charge carriers and resulting in severe non-radiative recombination.[32,33] Thus, elevating the formation energy of iodine vacancies and effectively minimizing their presence within the perovskite lattice are crucial strategies for reducing defect density and enhancing the stability of perovskite films. To assess the impact of FIPh-A on the suppression of iodine vacancies, we employed DFT calculations to determine the vacancy formation energy of perovskite after incorporating FIPh-A.[34,35] As shown in Figure 1b, the formation energy of iodine vacancy (V_I) increased from 4.86 eV to 5.19 eV by doping FIPh-A into perovskite, indicating that the incorporation of FIPh-A suppresses iodine vacancy formation through the synergistic interaction, which enhances the stability of the PbI_6 framework.

To validate the DFT results, X-ray photoelectron spectroscopy (XPS) characterization was performed on both with FIPh-A and control samples. As depicted in Figures 1c,d, the introduction of FIPh-A shifted the Pb 4f peak of the perovskite to a lower energy level by 0.2 eV, and the peaks associated with Pb^0 disappeared, indicating that the C═O group of FIPh-A interacted with uncoordinated Pb^{2+} in the perovskite film. Additionally, the fluorine atoms on the iodotetrafluorophenyl group may interact with Pb^{2+}, causing a shift in the lead peak position. To verify this hypothesis, we performed XPS characterization of pure FIPh-A and FIPh-A with PbI_2 samples to detect the binding energy changes of F element, as shown in Figure S11 (Supporting Information). The F 1s signal shifts from 686.20 eV in pure FIPh-A to 686.93 eV in FIPh-A with PbI_2. This shift is attributed to the coordination interaction between the fluorine atoms and Pb^{2+}. This finding suggests that Pb^{2+} can coordinate not only with carbonyl groups but also with the fluorine atoms on the iodotetrafluorophenyl group. The synergistic effects of carbonyl and fluorine atoms effectively passivate the uncoordinated Pb^{2+} in perovskite films. Such interaction helps stabilize the Pb—I octahedra in the perovskite structure and suppresses the formation of deep-level defects associated with Pb^0.

We also observed a shift in the I 3d peak to a lower energy level, corresponding to the formation of (NH···I) hydrogen

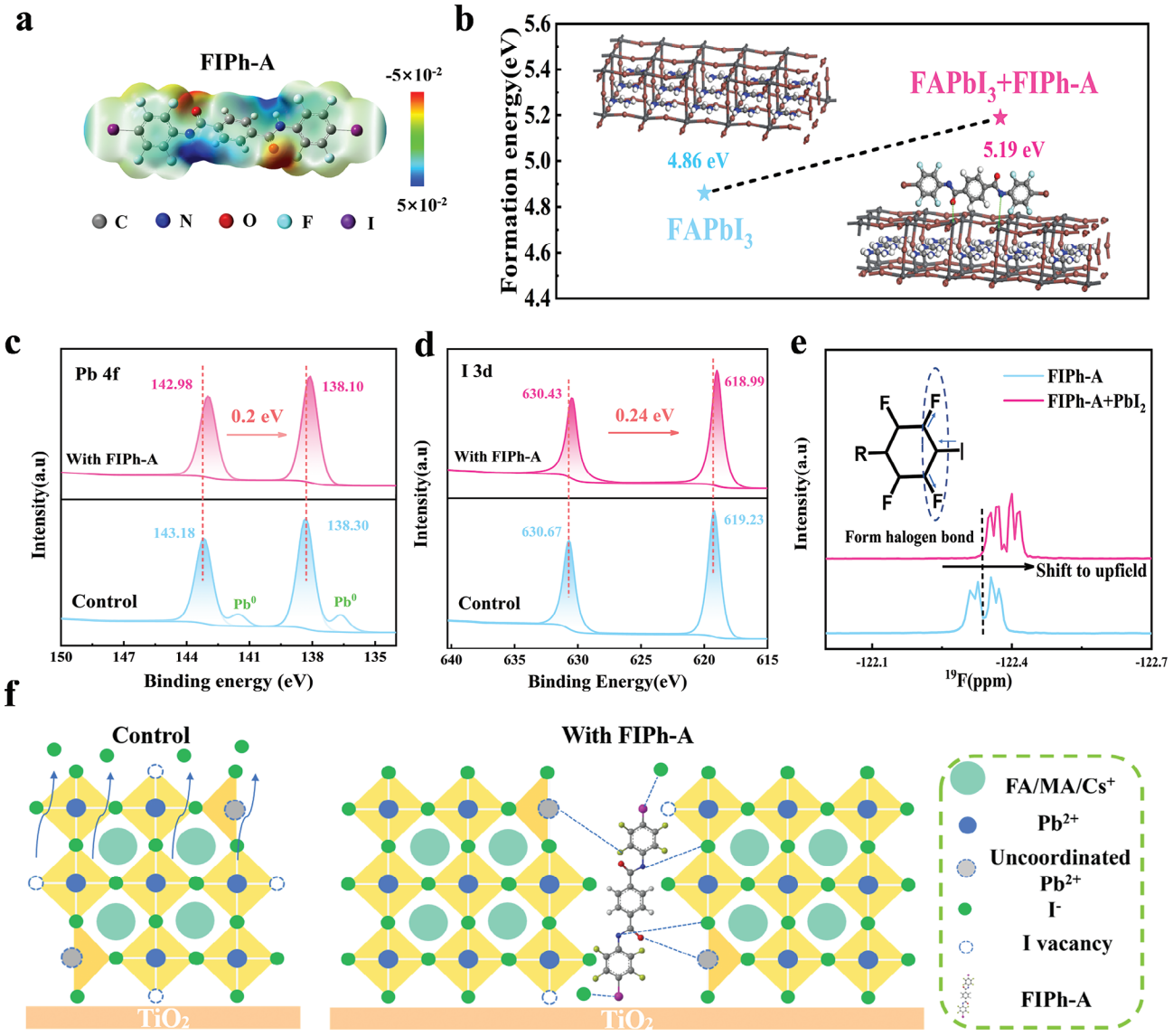

Figure 1. Mechanism of interaction between FIPh-A molecules and perovskite. a) The surface electrostatic potential distribution of FIPh-A. b) DFT calculation of formation energy of iodine vacancy (V_I). c) XPS spectrum of Pb 4f and d) I 3d regions. e) ^{19}F NMR spectrum of FIPh-A and FIPh-A with PbI_2 in DMSO-*d6* f) Schematic diagram of the interaction between FIPh-A and perovskite.

bonds.[36–38] Further verification was provided by nuclear magnetic resonance (NMR) spectroscopy, as shown in Figure S4 (Supporting Information). The NMR hydrogen spectrum of a mixture of PbI_2 and FIPh-A shifted lowfield compared to pure FIPh-A, confirming the formation of hydrogen bonds. Figure 1e presents the results of a ^{19}F NMR spectroscopy test, showing an upfield shift of the ^{19}F signal at 122 ppm after reaction with PbI_2. This shift, as previously reported,[39] indicates the formation of halogen bond (I···X^-) between the halogen bond donor (-C—I···) in the iodotetrafluorophenyl group from FIPh-A and the halide anion (X^-) from PbI_2. The highly electronegative fluorine atoms withdraw electron density from the aromatic ring, reducing electron density in the -C—I bond and creating a partial positive charge on the iodine atom. This anisotropic charge distribution results in a positive electrostatic potential along the -C—I bond axis, enabling the iodine to act as a halogen bond donor by interacting with electron-rich sites, such as halide anions (X^-). To support this analysis, we also conducted ^{13}C NMR tests, as shown in Figure S5 (Supporting Information). Previous studies have shown that the -C—I bond signal, originally between 73–75 ppm,[40] shifts downfield by 0.6 ppm, indicating reduced electron density at the carbon. Based on the NMR results of ^{13}C and ^{19}F exhibited above, we conclude that the halogen bond (I···X^-) between FIPh-A and PbI_2 is successfully established. Overall, as illustrated in Figure 1f, FIPh-A not only stabilizes the perovskite structure by forming coordination bonds with uncoordinated Pb^{2+} and hydrogen bonds with iodide anions of the $[PbI_6]^{4-}$ octahedra, but also immobilizes the I^- ions through halogen bonds, markedly increasing the threshold for ion migration.

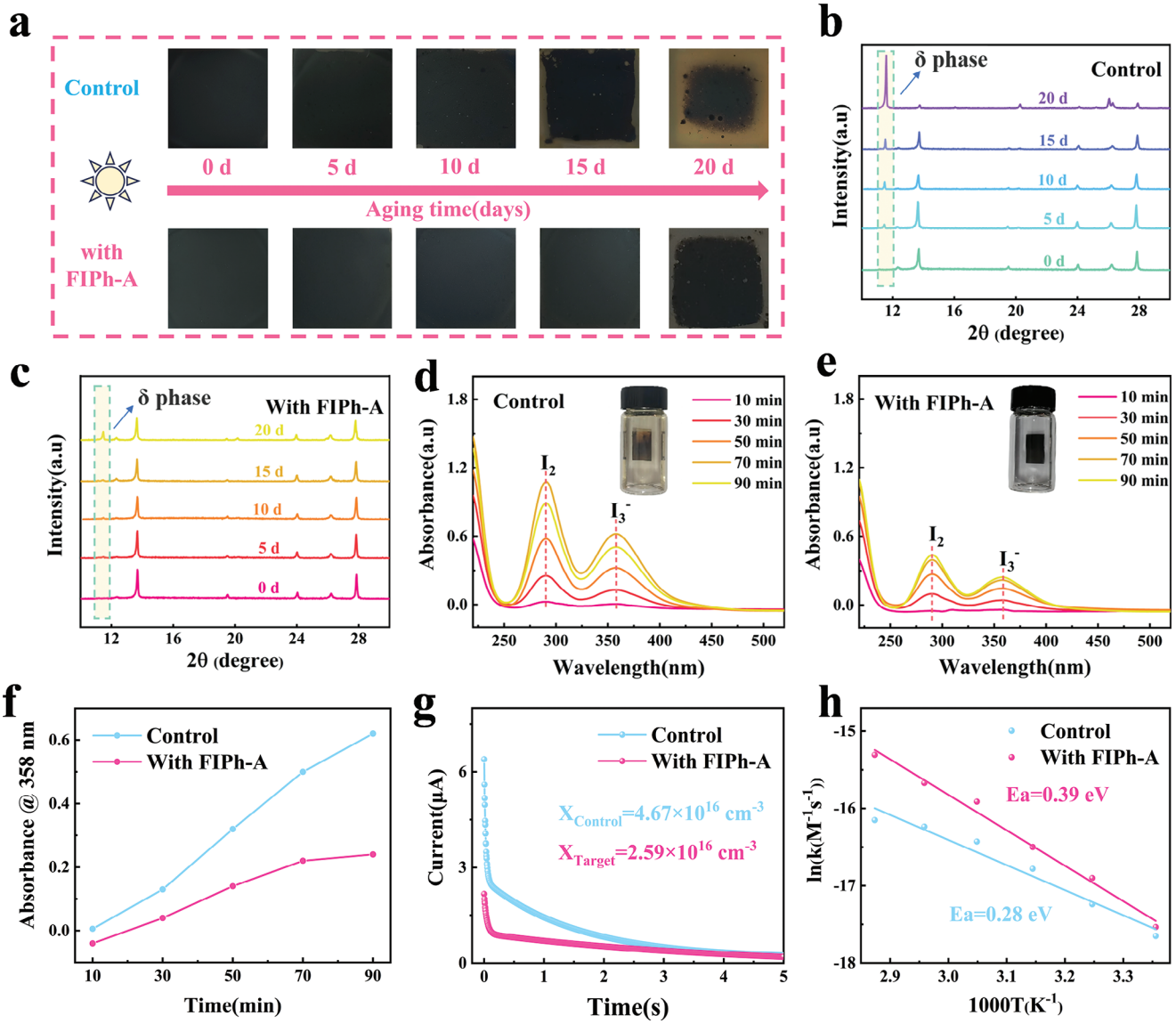

Figure 2. Enhanced light and thermal stability of perovskite films with FIPh-A. a) Photos of the control and with FIPh-A samples under continuous light aging at 55%–65% humidity. b), c) The evolution of X-ray diffraction (XRD) patterns of the control and with FIPh-A samples during light aging. d), e) UV-vis spectra of the control and with FIPh-A samples. f) Absorption peak at 358 nm observed in UV-vis spectra from 10 to 90 min. g) Transient ion migration current within 5s after a 1.5 V bias for the control and with FIPh-A samples. h) Temperature-dependent conductivity of the control and with FIPh-A samples, with temperature varying from 298 to 348 K.

To evaluate the impact of FIPh-A on stability, we conducted aging tests on perovskite films, both control and with FIPh-A, under continuous exposure to visible and UV light, electric field, as well as elevated ambient temperatures. For the illumination test, the films were placed in an air environment with 55%–65% RH and exposed to 1 sun solar intensity for 20 days. As shown in **Figure** 2a, the photographs of the tested samples indicate that compared to the control sample, with FIPh-A sample demonstrated better light stability; the film color remained unchanged until day 15 and only started to fade on day 20. To visually observe this process, we used an Optical Microscope (OM) to characterize the aging process. As shown in Figure S6a (Supporting Information), the black dots in the photos represent the δ-phase present in the perovskite films. Throughout the aging process, with FIPh-A sample showed no significant phase transition from 0–15 days; the film remained bright and uniformly luminescent until black dots appeared on day 20, indicating a phase transition. In contrast, the number of black dots continuously increased in the control sample, suggesting a subsequent δ-phase transition.

We continuously tracked changes in the optical properties of the perovskite films during aging using UV-vis spectroscopy, as shown in Figure S6b,c (Supporting Information). The control sample exhibited a noticeable reduction in absorption intensity and a shift in the absorption edge during aging, indicating a decline in perovskite optical properties and film degradation. By comparison, the absorption curve of the doped with FIPh-A

sample remained nearly unchanged over the 20 days of light exposure, indicating very stable optical properties.

As shown in Figures 2b,c, X-ray diffraction (XRD) reveals that the control sample developed a significant δ-phase peak at 11.5° during aging, indicating a marked phase transition after 20 days, particularly between days 15 and 20. This transition results from the combined effects of high humidity (55–65% RH) and light exposure. High humidity facilitates phase transitions by allowing moisture to form hydrogen bonds with perovskite cations like FA^+, disrupting ionic bonds with iodide ions and lowering the energy barrier for phase change. Simultaneously, light exposure induces halide ion migration, which destabilizes the lattice structure and further promotes phase transitions.[41,42] The interaction of high humidity and light accelerates degradation, leading to a pronounced α to δ-phase transition within 15 to 20 days. However, The FIPh-A-modified film showed no significant changes in peak position due to the synergistic effects of the carbonyl and amino groups, which, along with the halogen bond donors on the iodotetrafluorophenyl group, suppress light-induced ion migration and phase transitions in the perovskite film. This significantly enhances the film's photostability. Additionally, the fluorine atoms on the iodotetrafluorophenyl group provide hydrophobicity, improving the film's humidity stability.

Due to (UV) light irradiation potentially causing easier migration of I^- ions within the film and promoting their conversion to I_2 and I_3^-, we characterized the inhibiting effect of FIPh-A on the internal I^- ion migration and loss in the perovskite films by soaking the films in isopropanol (IPA) and irradiating them by 365 nm UV light. We used UV-vis to characterize the escaped halide ions in the solution to assess the inhibitory effect of FIPh-A on I^- migration. As shown in Figures 2d,e, two peaks appeared at 288 and 358 nm, representing the absorption peaks of I_2 and I_3^-, respectively. After 90 min of continuous UV irradiation, the peak intensities of I_2 and I_3^- from the perovskite film with FIPh-A are clearly lower than those from the pure perovskite film, indicating the inhibiting effect of FIPh-A on I^- escape. To gain a more intuitive understanding of this process, we plotted the intensity data of the peak at 358 nm, which indicates the escape of I_3^- from the aged films, as shown in Figure 2f. Our results demonstrate that the escaping amount of I_3^- in the perovskite film with FIPh-A is obviously lower than that in the control sample (pure perovskite film) after the same duration of UV aging. This observation further highlights the stabilizing role of the carbonyl and amino groups on the PbI_6 framework, as well as the efficient capture of I^- ions by the iodotetrafluorophenyl group. Thus, it can be concluded that the introduction of FIPh-A molecules enhances the stability of PbI_6 framework, significantly inhibiting the migration of I^- ions in the perovskite film.

The external electric field can also cause ion movement as reported in many published works.[43–46] Thus, to verify the effect of FIPh-A on inhibiting perovskite ion movement under an electric field, we applied a 1.5 V forward bias to the prepared perovskite devices in the dark state for 50 s to change the original distribution of moving ions under dark conditions, and then set the device to zero bias to allow for ion recovery movement. The "fast" ion migration current observed within seconds, as shown in Figure 2g, mainly results from halide ion migration within the perovskite.[47–49] The FIPh-A-modified device exhibited a smaller transient current, and by integrating the current versus time curve, we could calculate the number of ions moved within the device, as shown in Equation:

$$X = \frac{\int I\mathrm{d}t}{qSL} \tag{1}$$

where (I) represent the transient current, (q) is the elementary charge, (S) is the effective area of the active layer, and (L) is the thickness of the active layer. The ion concentration in the device with FIPh-A is 2.59×10^{16} cm^{-3}, significantly lower than 4.67×10^{16} cm^{-3} in the control group, indicating that ion migration in the FIPh-A-modified perovskite film was significantly inhibited. We then tested the activation energy of the devices by obtaining the conductivity at different temperatures using an electrochemical workstation and calculated the specific activation energy using the Arrhenius equation.[50,51] As shown in Figure 2h, the activation energy of the ion migration in perovskite devices with FIPh-A is increased from 0.28 to 0.39 eV, indicating that the incorporation of FIPh-A results in a higher ion migration barrier. These experimental and calculation findings confirm that FIPh-A can effectively stabilize the PbI_6 framework and inhibit ion migration in perovskite films, significantly enhancing the stability of both films and devices under continuous harsh environmental stress.

To investigate whether FIPh-A influences the crystallization of perovskite films, we characterized the control and with FIPh-A samples using scanning electron microscopy (SEM). As shown in **Figures 3**a,b, compared to the control sample, the cross-sectional morphology of the doped with FIPh-A sample displayed better crystallization, with crystal grain growth showing more evident orientation. The top view results in Figure S7 (Supporting Information) indicate that after the incorporation of FIPh-A, the average grain size of the sample increased from 432 to 561 nm. An increase in grain size is usually accompanied by a reduction in grain boundaries, which might help reduce defects in the perovskite films.

Subsequently, the crystallization of these perovskite films was analyzed using (XRD), as shown in Figures 3c,d. The intensity of the diffraction peaks in the FIPh-A-modified films was significantly enhanced, with narrower full width at half maximum in Table S2 (Supporting Information). The relative peak intensity ratio of (001)/PbI_2 increased from 6.20 to 15.84, indicating that the incorporation of FIPh-A helps suppress residual lead iodide in the perovskite films. These results suggest that FIPh-A not only contributes to the structural integrity of the perovskite by stabilizing the PbI_6 framework but also enhances the crystalline quality of the films. The improvement in crystal quality can also lead to a reduction in trap sites and potentially contribute to the observed increase in the stability and performance of PSCs.

The residual strain is the other important indicator for evaluating the crystallization quality of as-prepared perovskite films. Hence, the grazing incidence X-ray diffraction (GIXRD) was employed to further understand the impact of FIPh-A on the residual strain in the perovskite film crystallization process. These tests are illustrated in Figures 3e,f. By varying the incidence angle, we characterized the crystalline characterizes at different depths of the film. An increase in the incident angle provides deeper crystalline information. The results reveal that with increasing incident angles, the diffraction peaks of the control

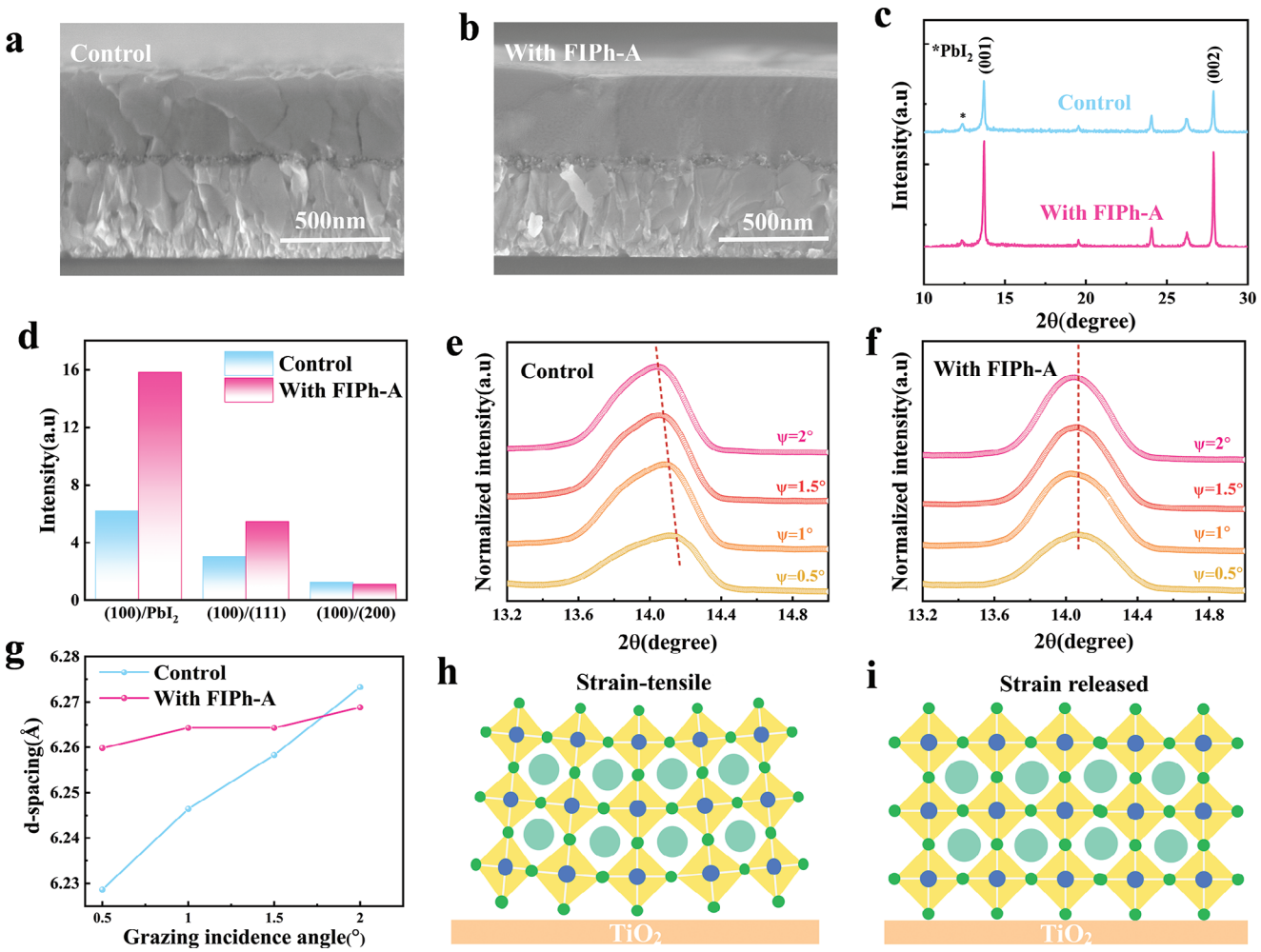

Figure 3. FIPh-A reduces residual strain in perovskite films. a), b) Cross-sectional SEM images of the control and with FIPh-A perovskite films. c) X-ray diffraction spectra of the control and with FIPh-A films. d) Peak intensity ratios of (100)/PbI_2, (100)/(111), and (100)/(200) for films w/wo FIPh-A. e), f) Diffraction peak shifts in GIXRD from a ψ value of 0.5° to 2° for the control and with FIPh-A samples. g) d-spacing values obtained from the (100) plane as a function of the incidence angle. h), i) Schematic diagrams of the strain in the control and with FIPh-A samples.

films shift towards smaller angles, indicating the presence of tensile strain within the perovskite film. In contrast, the diffraction peaks of the doped with FIPh-A perovskite hardly shift with changes in the incident angle. As shown in Figure 3g, the d-spacing of the control group continuously increases with higher incident angles, further confirming the influence of tensile stress. However, the d-spacing of the FIPh-A modified group remains relatively stable with increasing incident angles. This stability suggests that the incorporation of FIPh-A enhances the crystalline quality of the perovskite films, promotes grain growth orientation, and reduces residual film strain. The schematic diagrams of residual tensile strain (Figures 3h,i) clearly demonstrate how FIPh-A alleviates residual stress. This is attributed to the synergistic action of the C═O and -NH groups on FIPh-A, which stabilizes the Pb—I framework and promotes perovskite crystallization, thereby releasing strain. This result is consistent with the published reports.[52–54]

Improved crystalline quality indicates that the as-prepared film has fewer defects, which benefits to the transport of carriers. Therefore, we analyzed the carrier dynamics of the up-mentioned samples using steady-state photoluminescence (PL) and time-resolved photoluminescence (TRPL) spectroscopy. As illustrated in **Figure** 4a, both the control group and the group incorporating FIPh-A exhibit emission wavelengths near 800 nm, suggesting an approximate bandgap energy of 1.55 eV for these materials. This is consistent with our UV-vis data, as shown in Figure S9 (Supporting Information). The steady-state PL intensity of the FIPh-A modified perovskite increased, and the peak shifted blueward, indicating a reduction in internal defects and suppressed non-radiative recombination. Figure 4b shows the TRPL curves for both samples. We fitted the curves using a double-exponential Equation (2), deriving τ_1 and τ_2 values.[55] The τ_1 and τ_2 for the target sample were found to be 867.1 and 6631.7 ns, respectively, which are higher than those for the control sample at 712.9 and 5997.7 ns. A longer τ_1 indicates fewer defect recombination centers, thereby reducing the likelihood of non-radiative recombination. A longer τ_2 typically correlates with a lower non-radiative recombination rate and higher film quality, as detailed in Table

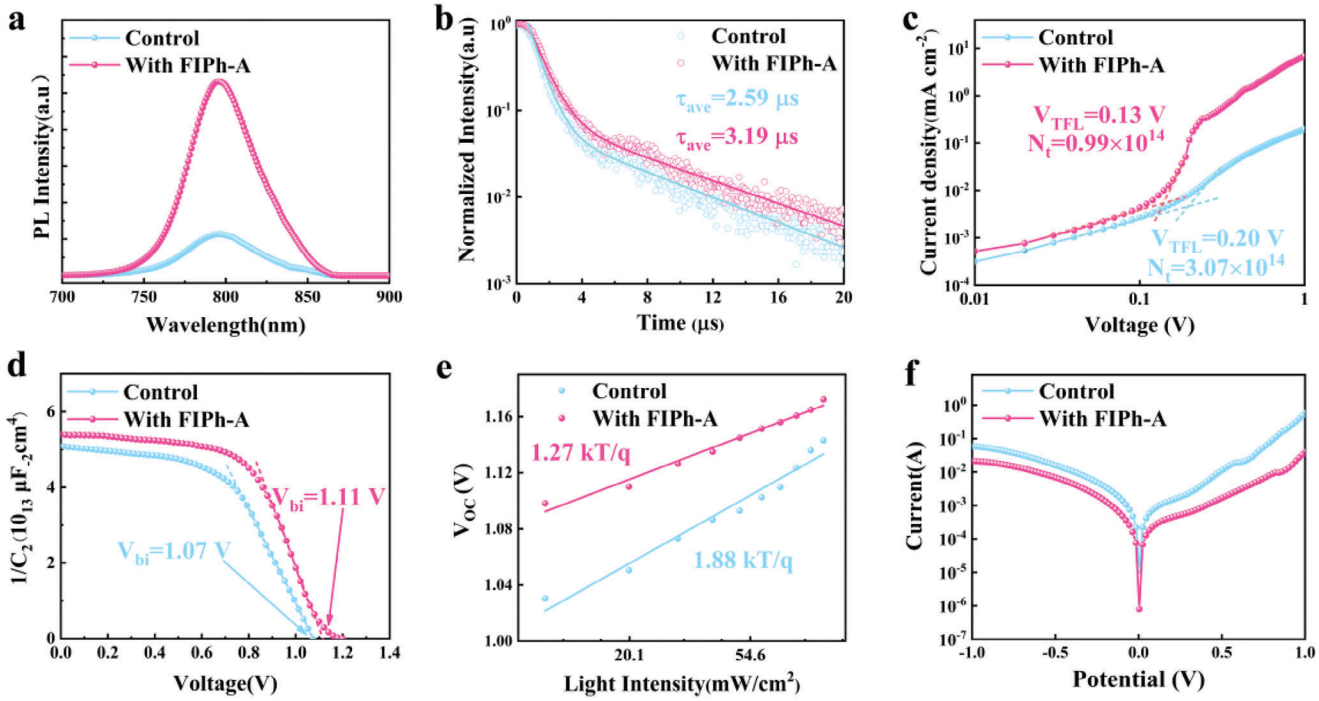

Figure 4. FIPh-A reduces defects in perovskite films. a) Steady-state photoluminescence (PL) spectra of the control and with FIPh-A samples. b) Time-resolved photoluminescence (TRPL) spectra of the control and with FIPh-A samples. c) Space-charge limited current (SCLC) test curves for the electron-only devices assembled by the control and with FIPh-A films. d) Mott-Schottky plots for the control and with FIPh-A devices. e) Ideality factor for the control and with FIPh-A devices. f) Dark current-voltage (*J-V*) curves for the control and with FIPh-A PSCs.

S1 (Supporting Information). Using the average lifetime Equation (3), we calculated the average carrier lifetimes (τ_{ave}) for the control and with FIPh-A samples as 2.59 and 3.19 μs, respectively. These results suggest that FIPh-A molecules help suppress internal defects and reduce carrier non-radiative recombination, which is associated with the enhanced crystalline quality and the effective passivation of defects by the functional groups on FIPh-A.

$$F\ (t) = A_1\ e^{\frac{t}{\tau_1}} + A_2 e^{\frac{t}{\tau_2}} \tag{2}$$

$$\tau_{ave} = \frac{\left(A_1\tau_1^2 + A_2\tau_2^2\right)}{A_1\tau_1 + A_2\tau_2} \tag{3}$$

To quantitatively assess the impact of FIPh-A on the defect density in perovskite films, we fabricated electron-only devices structured as FTO/TiO_2/Perovskite/ PCBM/Ag and conducted tests under dark conditions using the space-charge limited current (SCLC) method. The defect density was calculated based on the trap-filled limit voltage (V_{TFL}), using the following formula:[56]

$$N\ (t) = \frac{2\varepsilon_r\varepsilon_0 V_{TFL}}{(qL^2)} \tag{4}$$

where (ϵ_r) and (ϵ_0) represent the relative permittivity and vacuum permittivity respectively, (q) denotes the elementary charge, and (L) is the thickness of the perovskite film. As shown in Figure 4c, devices doped with FIPh-A exhibit a lower V_{TFL} value of 0.13 V, with a defect density of 0.99×10^{14} cm^{-3}, which is lower than the control group's V_{TFL} value of 0.2 V, with a defect concentration of 3.07×10^{14} cm^{-3}. This reduction indicates that FIPh-A significantly reduces the defect density in perovskite films through molecular interactions.

Then, we assembled these perovskite films into devices to characterize the changes in carrier transport in PSCs. The electrochemical impedance spectroscopy (EIS) of the device was measured at an external voltage of 1 V. As shown in Figure S8 (Supporting Information), the EIS spectra reveal that the recombination resistance of the FIPh-A-modified perovskite solar cells (11230 Ω) is higher than that of the control cells (6919 Ω), indicating a suppression of non-radiative recombination. We employed the Mott-Schottky method to test the capacitance-voltage (C-V) characteristics to determine the built-in electric field (V_{bi}) of the fabricated devices. The V_{bi} can be derived from the intercept on the x-axis of the Mott-Schottky plot. As shown in Figure 4d, it is apparent that the V_{bi} of the FIPh-A device is 1.11 V, which is higher than that of the control device at 1.07 V. The increased V_{bi} can be attributed to the reduction in perovskite charge defects. A higher V_{bi} is beneficial for the separation and extraction of carriers, thereby improving the fill factor (FF) and open-circuit voltage (V_{OC}) of PSCs.

We also measured the variation of V_{OC} with incident light intensity to deduce the ideality factor (n) of the testing devices.[57,58] As depicted in Figure 4e, the ideality factor of the FIPh-A modified device (n = 1.27 kT q^{-1}) is close to 1 kT q^{-1} and significantly lower than that of the control device (n = 1.88 kT q^{-1}), indicating that the addition of FIPh-A notably suppressed Shockley-Read-Hall (SRH) defect recombination in PSCs. Dark current-voltage

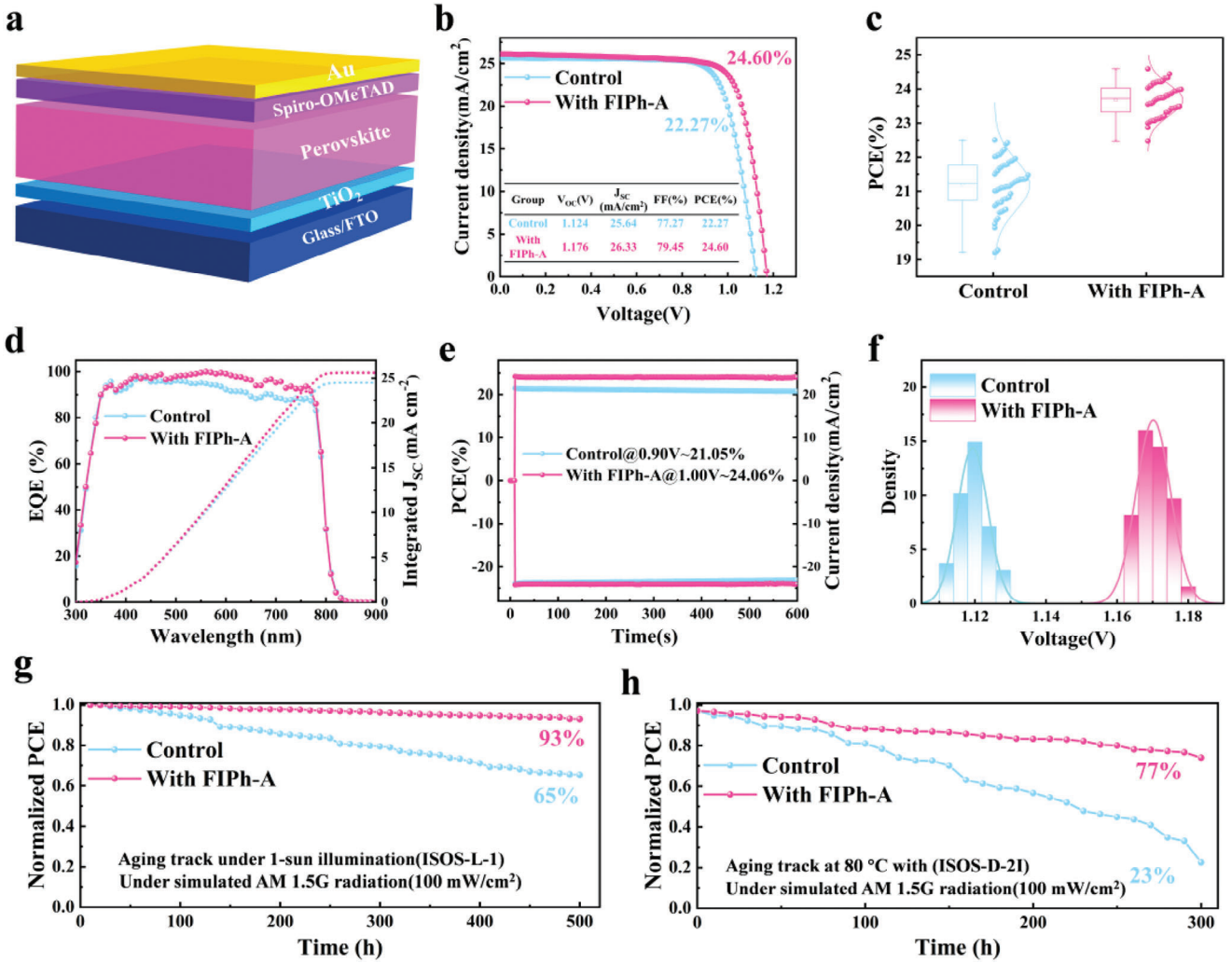

Figure 5. FIPh-A enhances efficiency and stability of PSCs. a) Schematic of the device structure. b) *J-V* curves of champion devices for the control and with FIPh-A. c) Efficiency distribution of devices for the control and with FIPh-A. d) EQE spectra and corresponding integrated *Jsc* for as-fabricated devices. e) Steady-state output of devices for the control and with FIPh-A. f) Open-circuit voltage distribution for devices of the control and with FIPh-A. g) Light stability of PSCs w/wo FIPh-A under continuous light illumination for 500 h. h) Thermal stability of PSCs w/wo FIPh-A at 80 °C without encapsulated for 300 h.

(*J-V*) curves of PSCs were recorded under dark conditions to document the dark current, as shown in Figure 4f. Compared to the control device, the PSC with FIPh-A exhibited significantly lower dark currents under both positive and negative biases, indicating much lower leakage currents and non-radiative recombination in the device. This is well consistent with the results of the ideality factor.

Higher crystalline quality, lower defects, less residual strain and more stable of PbI_6 framework of perovskite film are believed to be helpful for improving efficiency and stability of PSCs. Thus, PSCs with an n-i-p structure (FTO/TiO_2/Perovskite/Spiro-OMeTAD/Au) were assembled by these perovskite films to explore the changes of photovoltaic performance. As shown in **Figure** 5a, the schematic of the device structure is presented. PCE parameters of PSCs with different concentrations of FIPh-A were also exhibited in Figure S10(Supporting Information). The optimal doping concentration of FIPh-A had been determined to be 1 mg mL^{-1}, according to those efficiency parameters. Figure 5b shows the *J-V* curves of the devices for the control and with FIPh-A, obtained through reverse scanning. The control device exhibits an efficiency of 22.27%, with a short-circuit current density (J_{SC}) of 25.64 mA cm^{-2}, an open-circuit voltage (V_{OC}) of 1.124 V, and a fill factor (FF) of 77.27%. The PSC with FIPh-A achieves a champion PCE of 24.60%, with a J_{SC} of 26.33 mA cm^{-2}, V_{OC} of 1.176 V, and FF of 79.45%. The PCE of PSC with FIPh-A shows significant enhancement, particularly in V_{OC} and FF, which can be attributed to the synergistic effects of FIPh-A. FIPh-A with carbonyl, amino and iodotetrafluorophenyl groups can stabilize the PbI_6 framework and inhibit the ion migration, thereby minimizing the non-radiative recombination losses of carriers in PSCs. Figure 5c displays the statistical performance of 30 individual cells for both types of PSCs, showing that the devices with FIPh-A exhibit superior reproducibility compared to control devices. Figure 5d presents the external quantum efficiency (EQE)

spectra, where the integrated J_{SC} values for the control and FIPh-A modified PSCs are 24.49 and 25.60 mA cm^{-2}, respectively, consistent with the J_{SC} trends observed in the *J-V* curves. The steady-state PCE output (SPO) tracking results (Figure 5e) demonstrate that the steady-state PCEs for the control and the FIPh-A modified devices are 21.05% and 24.06%, respectively, confirming the reliability of the *J-V* characteristics. Figure 5f shows the open-circuit voltage distribution diagram. It can be observed that the V_{OC} of the device with FIPh-A is stably distributed ≈1.17 V, with peaks even reaching up to 1.18 V, significantly higher than that of the control devices.

The long-term stability of the as-fabricated PSCs was also evaluated, as shown in Figures 5g,h. For illumination tracking measurement, as shown in Figure 5g, after 500 h of continuous illumination following the ISOS-L-1 protocol, the PCE of the control device rapidly decreased to 65% of its initial value. In contrast, that of the device with FIPh-A shows superior stability, maintaining 93% of its initial value. For thermal aging tracking measurement, as shown in Figure 5h, after 300 h thermal aging at 80 °C following the ISOS-D-2I protocol,[59] the PCE of the control device rapidly decreased to 23% of its initial value, whereas the PCE of the device with FIPh-A exhibited better thermal stability, maintaining 77% of its initial value. The superior long-term stability of PSCs with FIPh-A, especially under harsh conditions, results from the significantly strengthened PbI_6 framework and effective suppression of ion migration, facilitated by the interaction between FIPh-A and perovskite films.

3. Conclusion

In summary, we designed and synthesized the FIPh-A molecule, utilizing additive engineering to stabilize the PbI_6 framework and capture I^- in perovskite, enhancing the crystalline quality of the perovskite films, suppressing I^- ion migration and loss, and reducing residual strain, thereby achieving high-efficiency and stable PSCs. The carbonyl (C═O) group and F atom in FIPh-A interacts with uncoordinated Pb^{2+}, while the -NH group forms (NH···I) hydrogen bonds with the I^- in $[PbI_6]^{4-}$ octahedra, stabilizing the PbI_6 octahedral structure through a synergistic effect that inhibits the escape of I^-. Additionally, the positively charged halogen bond donors on the iodotetrafluorophenyl group interacts with I^- to form halogen bonds, fixing these ions and significantly increasing the activation energy of I^- ions in perovskites. Moreover, the inclusion of FIPh-A molecules effectively reduces film residual strain, decreases defect density, and reduces carrier non-radiative recombination. Ultimately, devices treated with FIPh-A achieved a champion PCE of 24.60% with excellent light and thermal stability.

Supporting Information

Supporting Information is available from the Wiley Online Library or from the author.

Acknowledgements

This work is supported partially by the National Natural Science Foundation of China (Grant nos. 22103013, 52002070), Natural Science Foundation project of Fujian Province (No. 2021J01184, 2020J01197, 2023J01527).

Conflict of Interest

The authors declare no conflict of interest.

Data Availability Statement

The data that support the findings of this study are available from the corresponding author upon reasonable request.

Keywords

additive engineering, ion migration, long-term stability perovskite solar cells, stabilize PbI6 framework

Received: June 23, 2024
Revised: August 13, 2024
Published online:

[1] H. S. Kim, C. R. Lee, J. H. Im, K. B. Lee, T. Moehl, A. Marchioro, S. J. Moon, R. Humphry-Baker, J. H. Yum, J. E. Moser, M. Grätzel, N.-G. Park, *Sci. Rep.* **2012**, *2*, 591.
[2] M. Kim, G. H. Kim, T. K. Lee, I. W. Choi, H. W. Choi, Y. Jo, Y. J. Yoon, J. W. Kim, J. Lee, D. Huh, H. Lee, S. K. Kwak, J. Y. Kim, D. S. Kim, *Joule.* **2019**, *3*, 2179.
[3] Z. Liu, J. Hu, H. Jiao, L. Li, G. Zheng, Y. Chen, Y. Huang, Q. Zhang, C. Shen, Q. Chen, H. Zhou, *Adv. Mater.* **2017**, *29*, 1606774.
[4] X. Luo, X. Lin, F. Gao, Y. Zhao, X. Li, L. Zhan, Z. Qiu, J. Wang, C. Chen, L. Meng, X. Gao, Y. Zhang, Z. Huang, R. Fan, H. Liu, Y. Chen, X. Ren, J. Tang, C. H. Chen, D. Yang, Y. Tu, X. Liu, D. Liu, Q. Zhao, J. You, J. Fang, Y. Wu, H. Han, X. Zhang, D. Zhao, et al., *Sci. China: Chem.* **2022**, *65*, 2369.
[5] J. Park, J. Kim, H. S. Yun, M. J. Paik, E. Noh, H. J. Mun, M. G. Kim, T. J. Shin, S. I. Seok, *Nature.* **2023**, *616*, 724.
[6] M. Wang, Y. Lu, X. Huo, Q. Cai, Y. Yao, Y. Zhang, D. Song, Z. Xu, S. Chen, G. Chen, X. Li, D. Wei, *J. Power Sources.* **2023**, *561*, 232753.
[7] D. Wei, Q. Cai, S. Cai, Y. Wu, M. Wang, P. Cui, J. Ji, Z. Zhang, L. Yan, J. Zhang, J. Luo, X. Li, M. Li, *Nanoscale.* **2024**, *16*, 6669.
[8] Y. Wu, J. Zhang, J. Luo, M. Wang, S. Cai, Q. Cai, D. Wei, J. Ji, Z. Zhang, X. Li, *Appl. Surf. Sci.* **2024**, *662*, 160139.
[9] T. Yang, L. Gao, J. Lu, C. Ma, Y. Du, P. Wang, Z. Ding, S. Wang, P. Xu, D. Liu, H. Li, X. Chang, J. Fang, W. Tian, Y. Yang, S. Liu, K. Zhao, *Nat. Commun.* **2023**, *14*, 839.
[10] J. J. Yoo, G. Seo, M. R. Chua, T. G. Park, Y. Lu, F. Rotermund, Y. K. Kim, C. S. Moon, N. J. Jeon, J. P. Correa-Baena, V. Bulović, S. S. Shin, M. G. Bawendi, J. Seo, *Nature.* **2021**, *590*, 587.
[11] Y. Yao, M. Wang, Q. Cai, D. Wei, *Nanoscale.* **2022**, *14*, 7203.
[12] Q. Cai, Y. Yao, Y. Lu, M. Wang, Y. Zhang, D. Song, Z. Xu, X. Li, D. Wei, *Phys. Chem. Chem. Phys.* **2023**, *25*, 6955.
[13] N. R. E. Laboratory. Best Research-Cell Efficiency Chart. **2024**, https://www.nrel.gov/pv/cell-efficiency.html
[14] C. Eames, J. M. Frost, P. R. F. Barnes, B. C. O'Regan, A. Walsh, M. S. Islam, *Nat. Commun.* **2015**, *6*, 7497.
[15] Q. Feng, X. Huang, Z. Tang, Y. Hou, Q. Chang, S. Nie, F. Cao, X. Niu, J. Yin, J. Li, N. Zheng, B. Wu, *Energy Environ. Sci.* **2022**, *15*, 4404.
[16] G. Y. Kim, A. Senocrate, T. Y. Yang, G. Gregori, M. Grätzel, J. Maier, *Nat. Mater.* **2018**, *17*, 445.
[17] J. Liang, X. Hu, C. Wang, C. Liang, C. Chen, M. Xiao, J. Li, C. Tao, G. Xing, R. Yu, W. Ke, G. Fang, *Joule* **2022**, *6*, 816.
[18] Y. Chen, N. Li, L. Wang, L. Li, Z. Xu, H. Jiao, P. Liu, C. Zhu, H. Zai, M. Sun, W. Zou, S. Zhang, G. Xing, X. Liu, J. Wang, D. Li, B. Huang, Q. Chen, H. Zhou, *Nat. Commun.* **2019**, *10*, 1112.

[19] E. J. Juarez-Perez, L. K. Ono, M. Maeda, Y. Jiang, Z. Hawash, Y. Qi, *J. Mater. Chem. A.* **2018**, *6*, 9604.
[20] A. F. Akbulatov, S. Y. Luchkin, L. A. Frolova, N. N. Dremova, K. L. Gerasimov, I. S. Zhidkov, D. V. Anokhin, E. Z. Kurmaev, K. J. Stevenson, P. A. Troshin, *J. Phys. Chem. Lett.* **2017**, *8*, 1211.
[21] S. De Wolf, J. Holovsky, S. J. Moon, P. Loper, B. Niesen, M. Ledinsky, F. J. Haug, J. H. Yum, C. Ballif, *J. Phys. Chem. Lett.* **2014**, *5*, 1035.
[22] X. Li, S. Fu, W. Zhang, S. Ke, W. Song, J. Fang, *Sci. Adv.* **2020**, *6*, eabd1580.
[23] Y. Zhang, Q. Song, G. Liu, Y. Chen, Z. Guo, N. Li, X. Niu, Z. Qiu, W. Zhou, Z. Huang, C. Zhu, H. Zai, S. Ma, Y. Bai, Q. Chen, W. Huang, Q. Zhao, H. Zhou, *Nat. Photonics.* **2023**, *17*, 1066.
[24] X. Ren, J. Wang, Y. Lin, Y. Wang, H. Xie, H. Huang, B. Yang, Y. Yan, Y. Gao, J. He, J. Huang, Y. Yuan, *Nat. Mater.* **2024**, *23*, 810.
[25] X. Li, H. Yang, A. Liu, C. Lu, H. Yuan, W. Zhang, J. Fang, *Energy Environ. Sci.* **2023**, *16*, 6071.
[26] S. S. Chen, X. Xiao, H. Y. Gu, J. S. Huang, *Sci. Adv.* **2021**, *7*, eabe8130.
[27] X. Wang, D. Liu, R. Liu, X. Du, B. Zhang, X. Sun, C. Chen, Z. Li, Q. Zhao, Z. Shao, X. Wang, G. Cui, S. Pang, *Adv. Energy Mater.* **2023**, *13*, 2203635.
[28] Y. Cai, J. Cui, M. Chen, M. Zhang, Y. Han, F. Qian, H. Zhao, S. Yang, Z. Yang, H. Bian, *Adv. Funct. Mater.* **2021**, *31*, 2005776.
[29] P. Metrangolo, L. Canil, A. Abate, G. Terraneo, G. Cavallo, *Angew. Chem., Int. Ed.* **2022**, *61*, 202114793.
[30] R. A. Kerner, B. P. Rand, *J. Phys. Chem. Lett.* **2017**, *8*, 2298.
[31] W. Zhu, S. Wang, X. Zhang, A. Wang, C. Wu, F. Hao, *Small.* **2022**, *18*, 2105783.
[32] Z. Chen, G. Brocks, S. Tao, P. A. Bobbert, *Nat. Commun.* **2021**, *12*, 2687.
[33] S. Draguta, O. Sharia, S. J. Yoon, M. C. Brennan, Y. V. Morozov, J. S. Manser, P. V. Kamat, W. F. Schneider, M. Kuno, *Nat. Commun.* **2017**, *8*, 200.
[34] Z. C. Zhang, W. J. Chen, X. X. Jiang, J. L. Cao, H. D. Yang, H. Y. Chen, F. Yang, Y. X. Shen, H. Y. Yang, Q. R. Cheng, X. N. Chen, X. H. Tang, S. Q. Kang, X. M. Ou, C. J. Brabec, Y. W. Li, Y. F. Li, *Nat. Energy.* **2024**, *9*, 592.
[35] X. Y. Lu, K. X. Sun, Y. H. Wang, C. Liu, Y. Y. Meng, X. T. Lang, C. X. Xiao, R. J. Tian, Z. H. Song, Z. W. Zhu, M. Yang, Y. Bai, Z. Y. Ge, *Adv. Mater.* **2024**, *36*, 2400852.
[36] Y. H. Che, Z. K. Liu, Y. W. Duan, J. G. Wang, S. M. Yang, D. F. Xu, W. C. Xiang, T. Wang, N. Y. Yuan, J. N. Ding, S. Z. Liu, *Angew Chem Int Ed Engl.* **2022**, *61*, 202205012.
[37] B. B. Liu, X. D. Ren, R. Li, Y. Chen, D. M. He, Y. Li, Q. Zhou, D. Q. Ma, X. Han, X. X. Shai, K. Yang, S. R. Lu, Z. F. Zhang, J. Feng, C. Chen, J. H. Yi, J. Z. Chen, *Adv. Mater.* **2024**, *36*, 2312679.
[38] Y. M. Xu, X. Guo, Z. H. Lin, Q. R. Wang, J. Su, J. C. Zhang, Y. Hao, K. K. Yang, J. J. Chang, *Angew Chem Int Ed Engl.* **2023**, *62*, 202306229.
[39] X. L. Fu, T. W. He, S. F. Zhang, X. J. Lei, Y. Z. Jiang, D. Wang, P. C. Sun, D. B. Zhao, H. Y. Hsu, X. F. Li, M. Wang, M. J. Yuan, *Chem.* **2021**, *7*, 3131.
[40] A. Abate, M. Saliba, D. J. Hollman, S. D. Stranks, K. Wojciechowski, R. Avolio, G. Grancini, A. Petrozza, H. J. Snaith, *Nano Lett.* **2014**, *14*, 3247.
[41] D. W. deQuilettes, W. Zhang, V. M. Burlakov, D. J. Graham, T. Leijtens, A. Osherov, V. Bulović, H. J. Snaith, D. S. Ginger, S. D. Stranks, *Nat. Commun.* **2016**, *7*, 11683.
[42] K. Ho, M. Y. Wei, E. H. Sargent, G. C. Walker, *ACS Energy Lett.* **2021**, *6*, 934.
[43] E. Ruggeri, M. Anaya, K. Gałkowski, A. Abfalterer, Y. H. Chiang, K. Ji, Z. Andaji-Garmaroudi, S. D. Stranks, *Adv. Mater.* **2022**, *34*, 2202163.
[44] M. Saliba, E. Unger, L. Etgar, J. Luo, T. J. Jacobsson, *Nat. Commun.* **2023**, *14*, 5445.
[45] M. Vasiljevic, M. Kollár, D. Spirito, L. Riemer, L. Forró, E. Horváth, S. Gorfman, D. Damjanovic, *Adv. Funct. Mater.* **2022**, *32*, 2204898.
[46] D. Moia, I. Gelmetti, P. Calado, Y. Hu, X. Li, P. Docampo, J. de Mello, J. Maier, J. Nelson, P. R. F. Barnes, *Phys. Rev. Appl.* **2022**, *18*, 044056.
[47] Y. Deng, S. Xu, S. Chen, X. Xiao, J. Zhao, J. Huang, *Nat. Energy.* **2021**, *6*, 633.
[48] T. Tayagaki, A. Kogo, C. McDonald, V. Svrcek, T. Matsui, M. Yoshita, *IEEE J. Photovoltaics.* **2022**, *12*, 1170.
[49] Y. Yuan, J. Chae, Y. Shao, Q. Wang, Z. Xiao, A. Centrone, J. Huang, *Adv. Energy Mater.* **2015**, *5*, 1500615.
[50] D. Lin, T. Shi, H. Xie, F. Wan, X. Ren, K. Liu, Y. Zhao, L. Ke, Y. Lin, Y. Gao, X. Xu, W. Xie, P. Liu, Y. Yuan, *Adv. Energy Mater.* **2021**, *11*, 2002552.
[51] J. Mizusaki, K. Arai, K. Fueki, *Solid State Ionics.* **1983**, *11*, 203.
[52] Y. Che, Z. Liu, Y. Duan, J. Wang, S. Yang, D. Xu, W. Xiang, T. Wang, N. Yuan, J. Ding, S. Liu, *Angew. Chem., Int. Ed.* **2022**, *61*, 202205012.
[53] C. Tian, B. Li, Y. Rui, H. Xiong, Y. Zhao, X. Han, X. Zhou, Y. Qiu, W. An, K. Li, C. Hou, Y. Li, H. Wang, Q. Zhang, *Adv. Funct. Mater.* **2023**, *33*, 2302270.
[54] H. Wang, J. Du, X. Li, H. Duan, S. Yang, D. Han, J. Yang, L. Fan, F. Wang, L. Yang, *Chem. Eng. J.* **2022**, *450*, 137990.
[55] H. Bi, X. Zuo, B. Liu, D. He, L. Bai, W. Wang, X. Li, Z. Xiao, K. Sun, Q. Song, Z. Zang, J. Chen, *J. Mater. Chem. A.* **2021**, *9*, 3940.
[56] C. Ma, M. C. Kang, S. H. Lee, S. J. Kwon, H. W. Cha, C. W. Yang, N. G. Park, *Joule.* **2022**, *6*, 2626.
[57] W. Meng, Y. Hou, A. Karl, E. Gu, X. Tang, A. Osvet, K. Zhang, Y. Zhao, X. Du, J. Garcia Cerrillo, N. Li, C. J. Brabec, *ACS Energy Lett.* **2019**, *5*, 271.
[58] Y. Meng, C. Liu, R. Cao, J. Zhang, L. Xie, M. Yang, L. Xie, Y. Wang, X. Yin, C. Liu, *Adv. Funct. Mater.* **2023**, *33*, 2214788.
[59] M. V. Khenkin, E. A. Katz, A. Abate, G. Bardizza, J. J. Berry, C. Brabec, F. Brunetti, V. Bulovic, Q. Burlingame, A. Di Carlo, R. Cheacharoen, Y. B. Cheng, A. Colsmann, S. Cros, K. Domanski, M. Dusza, C. J. Fell, S. R. Forrest, Y. Galagan, D. Di Girolamo, M. Graetzel, A. Hagfeldt, E. von Hauff, H. Hoppe, J. Kettle, H. Koebler, M. S. Leite, S. Liu, Y. L. Loo, J. M. Luther, et al., *Nat. Energy.* **2020**, *5*, 35.